Dynamics of probe particles in polymer solutions and gels

J. C. Reina, R. Bansil* and C. Koňák†
Center for Polymer Studies and Department of Physics, Boston University, Boston, Massachusetts, USA
(Received 20 January 1989; revised 26 May 1989; accepted 9 June 1989)

The dependence of the dynamics of probe particles in polyacrylamide solutions and gels as a function of crosslink content, scattering angle and size of the probe is studied using photon correlation spectroscopy. Several fitting methods were applied to the auto-correlation functions obtained from samples ranging through the gelation threshold. We observed a complex dynamical behaviour ranging from the purely translational diffusion of the probes in the medium to a relaxational behaviour associated with the local movement of the latex particles in the gel. In addition, in samples which are beyond the gelation threshold, where a large fraction of the latex particles are immobilized, we observe a coupling between the movement of the particle and the collective diffusion mode of the gel network itself. Our results show that the crossover from diffusional to relaxational behaviour depends on the length scale over which the movement is probed and the mesh size of the network.

(Keywords: polyacrylamide solutions; probe particles; dynamics; photon correlation spectroscopy)

INTRODUCTION

The subject of diffusion in random media has recently received a lot of attention[1]. Polymer gels provide an excellent example of such a system. The diffusional properties of polymer solutions and gels can be easily investigated by means of quasielastic light scattering of probe particles suspended in the polymeric medium[2–4]. This technique[5] has been extensively used to study probe diffusion in polymer solutions. For example, Phillies *et al.*[6] have developed a scaling relation for the diffusion of probes in semidilute polymer solutions as a function of the polymer molecular weight, concentration and the radius of the probe. Probe dynamics is more complex in the gel phase than in semidilute solutions because the movement of the particle is influenced not only by the viscosity of the solution but also by the viscoelastic effects in the gel and the network structure. The problem of probe diffusion in polymer gels[7–9] and porous glasses[10] has only recently been investigated by quasi-elastic light scattering. Previously sedimentation techniques have been used to investigate this problem[11]. Allain *et al.*[7] have studied diffusion of monodispersed polystyrene latex microspheres in polyacrylamide during the course of the gelation reaction. They observed a broadening of the distribution of relaxation rates at the gel threshold and a departure from single exponential behaviour at larger decay times. This non-single exponential nature of the intensity auto-correlation function near and beyond the gelation threshold was also evident in our previous experiments[9,12]. In an effort to understand this complex dynamics, we report a detailed analysis of the intensity and electric field auto-correlation functions measured over several decades of sampling time from latex particles in polyacrylamide solutions and gels as a function of crosslink content and the scattering vector **K**.

We observed a complex dynamical behaviour ranging from the purely translational diffusion of the probes in the medium to a relaxational behaviour associated with the local movement of the latex particles in the gel. In addition, in samples which are beyond the gelation threshold where a fraction of the latex particles are immobilized, we observe a coupling between the particles movement and the collective diffusion mode of the gel network itself. Our results show that the crossover from diffusional to relaxational behaviour depends on the length scale over which the movement is probed and the mesh size of the network.

EXPERIMENTAL

The samples used in this experiment are polyacrylamide gels or solutions made by co-polymerizing acrylamide (AAm), and bisacrylamide (Bis), using ammonium persulphate as initiator (40 mg/100 ml), and tetra-ethyl-methylene-diamine (160 μl)/100 ml as catalyst in presence of water. A series of samples with a total monomer concentration, [AAm] + [Bis] = 2.5% (w/v), but differing in the crosslink content, $f_{Bis} = [Bis]/([Bis] + [AAm])$, varying from 0% (linear polymer), through the gel threshold sample f_{Bis}^c, to 5% (strong gel) at increments of 0.25%, were prepared using standard methods[13]. By visual observation as well as by previous results we could identify $f_{Bis}^c = 1.5\%$, as the gel threshold sample. For $f_{Bis} < f_{Bis}^c$ the sample is a solution whereas above 1.5% it is a gel. Prior to the initiation of the polymerization process, a small amount ($< 100\ \mu$l) of highly monodispersed aqueous suspension of polystyrene latex spheres (Polysciences, 2.5% solids-latex), of either 50 ± 5 nm or 100 ± 10 nm in diameter (d), was added to each pre-gel mixture. The amount of latex suspension

* To whom correspondence should be addressed
† Permanent address: Institute for Macromolecular Chemistry, Prague, Czechoslovakia

0032-3861/90/061038-07

used was varied such that the latex particles scattering intensity was adjusted to be ≈ 100 times larger than that of the pure polymer solution and gel. This typically corresponds to about 0.03% latex particles by volume. Because of the very large scattering intensity from the latex particles the correlation functions have no significant contribution due to the movement of the polymer chains or gels, except when a large trapping of the probes occurs and thus we can interpret the correlation functions in terms of the movement of the probes. All monomer solutions were carefully filtered using 0.22 μm Millipore filters, to minimize the dust factor, which was therefore not considered.

The absence of chemical bond formation or adsorption of polymer on probes and/or aggregation of the probes was carefully tested both in water solutions (with detergent) and in polymer solutions by measuring the apparent hydrodynamic radius over several weeks. We have found no change in the apparent hydrodynamic radius over this prolonged period of time, within experimental error. Actually, we observed that the latex is more stable against aggregation when incorporated in polyacrylamide gels. Also we compared two gel and latex samples, one with the detergent Triton X-100 added and one without and found no change in the apparent hydrodynamic radius, suggesting that the latex probes do not aggregate in polyacrylamide.

Measurements of the scattered light intensity auto-correlation functions, $C(\tau)=\langle n(t+\tau)n(t)\rangle$, where n is the number of photocounts, at a constant temperature of 20.0 ± 0.01°C, through scattering angles ranging from 15° to 138°, (290 nm $\geqslant 1/\mathbf{K} \geqslant$ 40 nm), were performed using a standard laser light multi-angle spectrometer with a 15 mW He-Ne laser (6328 Å) and a 64 real-time channels, multi-bit Langley Ford 1096 correlator. Measurements of multiple sample times correlation functions were performed on a Brookhaven Instruments (Model BI-2030AT) 72-channel, digital correlator. The measurements on gels without latex required the use of an argon-ion laser with a power at the sample of 300 mW, with the 5145 Å laser line.

In view of the previously published results[7,9] concerning non-single exponentiality of the intensity auto-correlation functions, our measurements extend over a much larger dynamical range than done previously. Three different methods were used to extend the dynamical range: multi-block, which involved multiplexing the available real-time channels, to generate a total of 1024 channels, extending over three orders of delay time; semi-log composite, which involved measuring several correlation functions with increasing sample times and then forming out of them a composite which covered more than 3.5 orders; and multi-sampling time, which involved splitting the available real-time channels into four separate groups of sixteen channels, each with different sample times, covering 4.5 orders. The first two methods were done with the Langley Ford correlator, whereas the real-time extended correlation functions were measured with the Brookhaven correlator.

Figure 1 shows data measured at 90° on the same sample, with $f_{\text{Bis}}=2\%$ and 50 nm probes. The quantity plotted is the normalized baseline subtracted intensity auto-correlation function, i.e. $\mathscr{G}^{(2)}(\tau)\equiv[C(\tau)-C(\infty)]/C(0)$, where $C(\infty)$ is the theoretical baseline or $\langle n\rangle^2$. As can be seen by comparing the correlation functions for the same time scale for all methods, the differences between

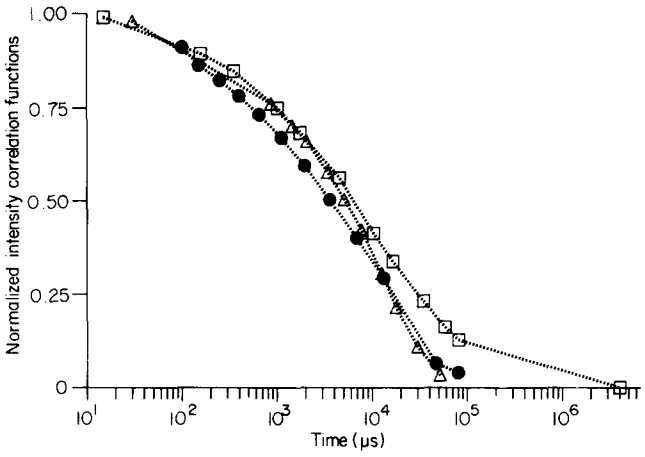

Figure 1 The normalized intensity correlation functions, $[C(\tau)-C(\infty)]/C(0)$, from a $f_{\text{Bis}}=2.0\%$ sample, with 50 nm probes measured at 90°. (●), Multiblock: Multiplexing the available real-time channels, to generate a total of 1024 channels, extending over three orders of delay time; (△), Semi-log composite: Measuring several 'normal' correlation functions with increasing sample times and then forming out of them a composite which covered more than 3.5 orders; and (□), Multi-sampling time: Splitting the available real-time channels into four separate groups of sixteen channels, each with different sample times, covering 4.5 orders

them are small and the effective decay constants obtained from them by an analysis differ by less than 10%[12]. In this paper we present results mostly from the multi-sample time correlation functions because they can be obtained faster and their dynamical range is sufficiently large, although results from multi-block correlation functions obtained from the samples in the solution regime are also presented.

DATA ANALYSIS

In the homodyne mode the measured correlation function, $C(\tau)$ can be written in terms of the electric field correlation function $g^{(1)}(\tau)$ by using Siegert's relation

$$C(\tau)=C(\infty)[1+b|g^{(1)}|^2] \qquad (1)$$

where $b=1-[C(0)/C(\infty)]$ is the term due to the non-ideal point detector. We have applied several data analysis methods to determine the decay constants of the correlation functions. These include force fits of $g^{(1)}(\tau)$ to a single exponential; cumulant analysis of the intensity correlation function, $C(\tau)$; double exponential fit to $g^{(1)}(\tau)$; Laplace inversion techniques to determine a continuous distribution of decay constants performed by the Ostrowsky–Pike exponential sampling technique[14,15] and the non-linear least square method.

RESULTS AND DISCUSSION

Figure 2 shows the measured intensity correlation functions, represented by the decaying curves, normalized to unity at $\tau=0$, i.e. $C(\tau)/C(0)$, from samples with 50 nm probes and increasing f_{Bis}: 1.3% (pre-gel), 1.5% (threshold), 1.7% and 2.0% (gelled) and 3.5% (well-gelled). Two features are obvious from this plot: $C(\tau)$ decays most slowly in the vicinity of the gel threshold; and the dynamic amplitude decreases as f_{Bis} increases, which is evidenced by the increasing baseline. The normalized baseline, $C(\infty)/C(0)$, increases from ≈ 0.67 in the solution samples to ≈ 0.96 in the well gelled

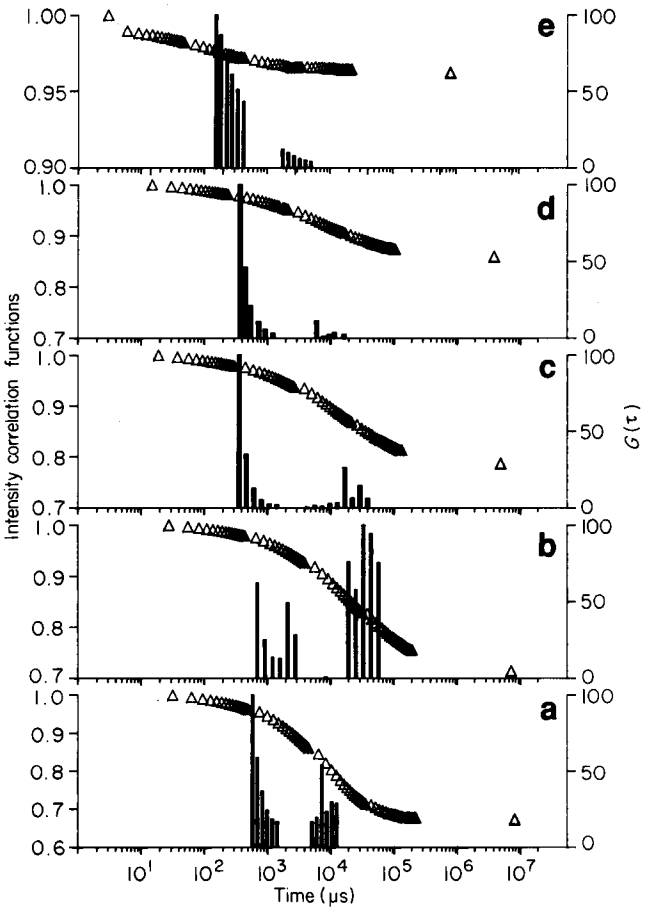

Figure 2 Normalized intensity correlation functions $C(\tau)/C(0)$, represented by the decaying curves, for 50 nm probes in samples with increasing f_{Bis}: (a) 1.3% (pre-gel); (b) 1.5% (threshold); (c) 1.7% (gelled); (d) 2.0% (gelled); and (e) 3.5% (well-gelled). Also shown are the histograms of the distribution functions $G(\tau)$, of decay rates obtained by the exponential sampling Laplace inversion technique, obtained from the corresponding correlation functions. For all samples shown (f_{Bis}=1.3, 1.5, 1.7, 2, 3.5%, with 50 nm latex probes, 90° scattering angle), the slow and fast modes are separated at least by an order of magnitude, and the relative contributions of the slow and fast modes depend on f_{Bis}

samples, which is interpreted as arising from the trapping of some of the probe particles in the gel samples[9]. (For comparison, 50 nm latex particles in water have a normalized baseline of 0.65).

The occurrence of trapped particles acting as local oscillators may cause partial heterodyning in the well gelled samples. For samples with $f_{Bis}<2.0\%$ the fraction of trapped particles is relatively small and heterodyning is insignificant. The effect of partial heterodyning can be estimated using the results of Oliver[16]. As shown there and by Bloomfield[17] the intensity auto-correlation function in the case of partial heterodyning should be written with mixed terms representing the homodyne terms from the randomly diffusing probes and the heterodyne terms due to the trapped particles, as follows

$$g^{(2)}(\tau)=1+(2\langle n\rangle_s\langle n\rangle_o/(\langle n\rangle_s+\langle n\rangle_o)^2)g^{(1)}(\tau)+(\langle n\rangle_s/(\langle n\rangle_s+\langle n\rangle_o))^2|g^{(1)}(\tau)|^2 \quad (2)$$

The error in the effective decay rate caused by neglecting the cross term (see equation (75) of ref. 16) is about 15% when the ratio between local oscillator (in our case the trapped particles) count-rate per sample time, $\langle n_o\rangle$, over the average signal $\langle n_s\rangle$, is 0.1 and increases to ≈30% as this ratio increases to 0.3 (see Figure 20 of ref. 16). As shown in *Figure 2* the increase in the normalized baseline from the solution to the well gelled samples (where the trapping would be the greatest) is ~0.3, which gives $\langle n_o\rangle/\langle n_s\rangle\approx 0.3/0.7\approx 0.4$ and thus implies that the decay constant obtained by using the homodyne assumption for the well gelled samples is about 40% off. Because the decay constants change by orders of magnitude when f_{Bis} increases the overall interpretation of our results is not affected by this partial heterodyning. However, it should be borne in mind that the decay constants for the extremely well gelled samples are imprecise to within a factor of 1.4.

It was found that for samples well below the gel threshold correlation functions were single exponential in character; for $f_{Bis}=0\%$ this was verified over the entire 4.5 decades of sampling time, whereas for samples up to $f_{Bis}=0.75\%$ the departure from single exponential was very slight. In fact for samples with $f_{Bis}<0.75\%$ a double exponential fit produced two decay modes which overlapped within error bars of the fit. Thus for the solution samples the single exponential and cumulant fits work well. For purposes of estimating the effective decay rate we also applied a fourth order cumulant analysis to $C(\tau)$ obtained from samples in the vicinity of and beyond the gel threshold. Because these data are obviously non-single-exponential a cumulant analysis here only provides an estimate of the effective decay constant and therefore we cannot base any interpretation of the mechanics of probe diffusion on the results of the cumulant method.

At $f_{Bis}>0.75\%$ small deviations from single exponentiality became obvious until at $f_{Bis}=1.5\%$ which corresponds to the gel threshold sample, the non-single exponential behaviour becomes very clear. Thus for these samples single exponential fits are inappropriate. In order to assess the nature of the distribution of decay rates we tried Laplace inversion techniques which allowed us to estimate the distribution function of decay times $G(\tau)$. The Ostrowsky–Pike exponential sampling and the non-linear least squares methods both produced a bimodal distribution. The histograms of the distributions obtained by the exponential sampling method from samples with increasing f_{Bis} are also shown in *Figure 2*. In all cases the slow and fast modes are separated at least by an order of magnitude, and the relative contribution of the slow and fast modes depend on f_{Bis}.

Because the distribution found by the exponential sampling method was found to be bimodal for all correlation functions, a double exponential force fit can be taken as a reasonable model to parameterize the data.

Figure 3a shows a semilog plot of a typical multi-sampling time correlation function *versus* delay time which was measured from a $f_{Bis}=1.6\%$ sample with 50 nm latex probes at an angle of 90° using the Brookhaven correlator. *Figure 3b* shows the distribution function $G(\tau)$, obtained by the exponential sampling method. As stated earlier, the distribution of relaxation rates is clearly bimodal. *Figure 3c* shows the positions of the two modes obtained from a double exponential fit to the electric field correlation function, $g^{(1)}(\tau)$, i.e. $g^{(1)}(\tau)=A_s\exp(-\Gamma_s t)+A_f\exp(-\Gamma_f t)$, where Γ_s, Γ_f and A_s, A_f are the apparent decay rates and amplitudes of the slow and fast modes, respectively, with the condition $A_f+A_s=1$. The amplitudes A_f and A_s were corrected for Mie scattering using the programs of ref. 15 so that the

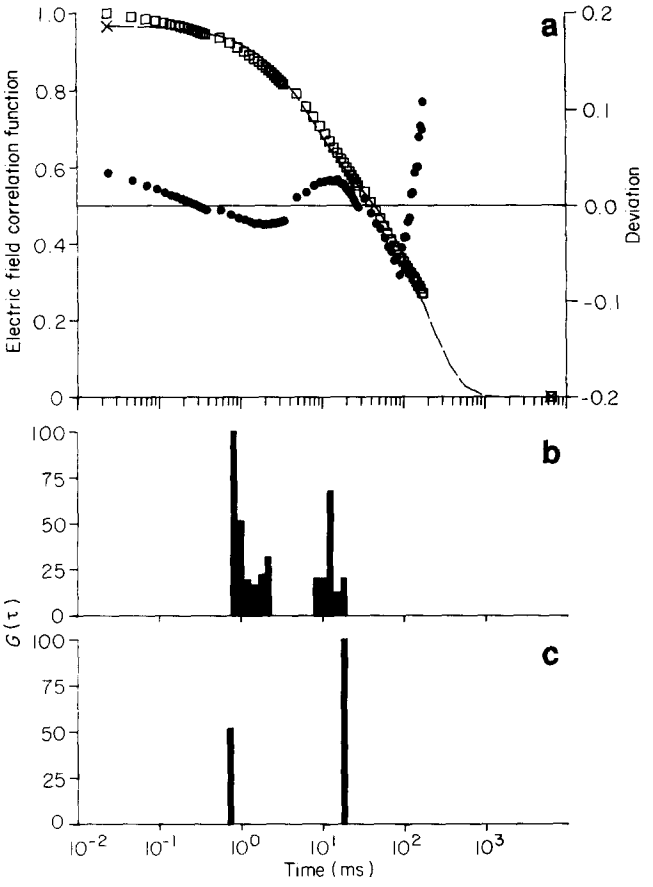

Figure 3 (a) Semilog plot of a typical multi-sampling time correlation function from a $f_{Bis} = 1.6\%$ sample with 50 nm latex probes at an angle of 90°. □, Measured data; – – –, best double exponential fit as explained in the text; ●, percent deviation of the residuals in the double exponential fit. (b) Distribution function $G(\tau)$, obtained by the exponential sampling method, corresponding to the extended correlation function of *Figure 3a*. (c) The two modes obtained in the double exponential fit of the same correlation function

K dependence of the quantities A_f and A_s reflects only the length scale dependence of the probe movement on different length scales (the correction is very small as expected for small size particles). The decay rates are in reasonable agreement with the peak positions of the two groups of modes in the exponential-sampling analysis. The best double exponential fit is represented in *Figure 3a* by the dashed fitting curve. The residuals of this fit lie within 5% of $g^{(1)}(\tau)$ during most of the process except in the last few channels. Therefore, as a first approximation, a double exponential fit can be used to parameterize the measured correlation functions.

To summarize these results, for samples with $f_{Bis} \leqslant 0.5\%$ a cumulant analysis is adequate to interpret the correlation functions, but as we approach the critical concentration, $f_{Bis} \geqslant 0.75\%$, a cumulant analysis becomes poorer, whereas a double exponential, and an exponential-sampling analysis produced good fits to the data.

Results of the double exponential analysis

Analysis of the dependence of the parameters of the double exponential provide some understanding of the dynamics of probe movement in gels and pre-gel solutions.

The results of the double exponential analysis are summarized in *Figures 4* and *5*. *Figure 4a* shows the apparent decay rates of the two modes, Γ_f and Γ_s, as a function of the crosslink concentration f_{Bis}, for correlation functions measured at a fixed scattering vector $\mathbf{K} = 1.87 \times 10^5\ cm^{-1}$, corresponding to 90°, for samples with 50 nm latex probes. Also shown in *Figure 4a* is the first cumulant obtained from a fourth order cumulant fit of the data. Qualitatively, similar results were obtained with the 100 nm probes.

As mentioned earlier, the normalized baseline, which is a measure of the relative amounts of the dynamic and the static light scattering intensity, depends strongly on f_{Bis} and **K**. We have suggested in a previous paper[9] how this dependence can be related to the fraction of moving particles f_{mov}, (see equation (4) in ref. 9). The dependence of normalized theoretical baseline $C(\infty)/C(0)$ on f_{Bis} for fixed **K** is shown in *Figure 4b*.

Figure 4b shows clearly that for $f_{Bis} < f_{Bis}^c$ the normalized dynamical amplitude $[1 - C(\infty)/C(0)] \equiv 1 - B$ is independent of f_{Bis}, implying that there is no significant trapping of the latex probes, whereas after the sol–gel transition at f_{Bis}^c the normalized dynamic amplitude decreases monotonically. This is related to the occurrence of trapped probe particles and using the results of ref. 9 at $f_{Bis} = 3\%$, about 90% of the probes are trapped.

This decrease in $1 - C(\infty)/C(0)$ and the observation that the apparent decay rates of both the slow and fast modes go through a minimum at f_{Bis}^c (see *Figure 4a*) strongly suggest that the mechanism governing probe movement is qualitatively different in the sol phase, $f_{Bis} < f_{Bis}^c$ (region I of *Figure 5*) and in the gel phase, (region II of *Figure 5*), $f_{Bis} > f_{Bis}^c$.

In region I for f_{Bis} well below f_{Bis}^c the correlation function can be described by a single exponential decay very well. This behaviour is characteristic of probe diffusion in semi-dilute solutions and one expects the Stokes–Einstein relation to be valid, i.e., $\mathcal{D} = kT/3\pi\eta d$,

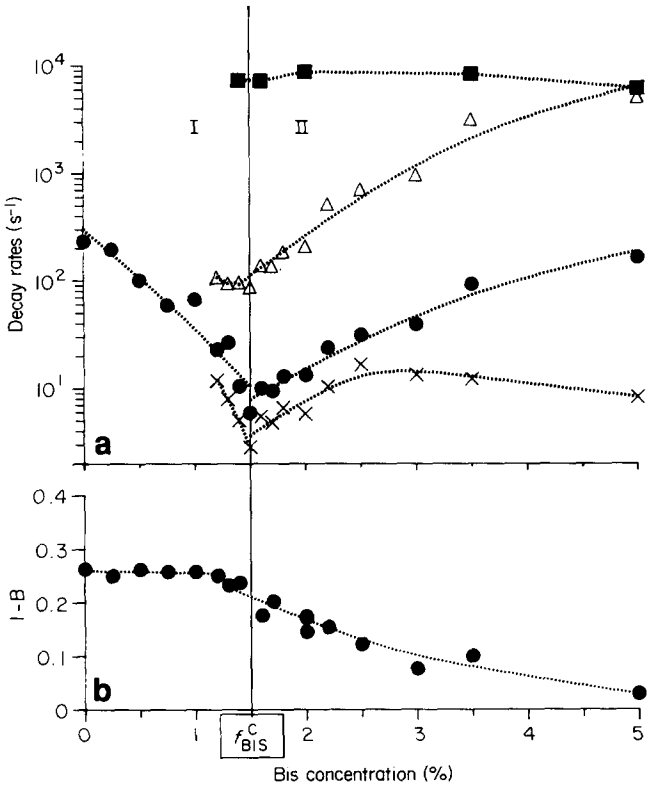

Figure 4 Crosslink content dependence of (a) apparent decay rates: ×, slow mode, Γ_s; △, fast mode, Γ_f; ●, first cumulant, K_1; ■, decay rate measured from gels without probes using an argon-ion laser as described in text. (b) Ratio of the amplitudes of the fast and slow modes

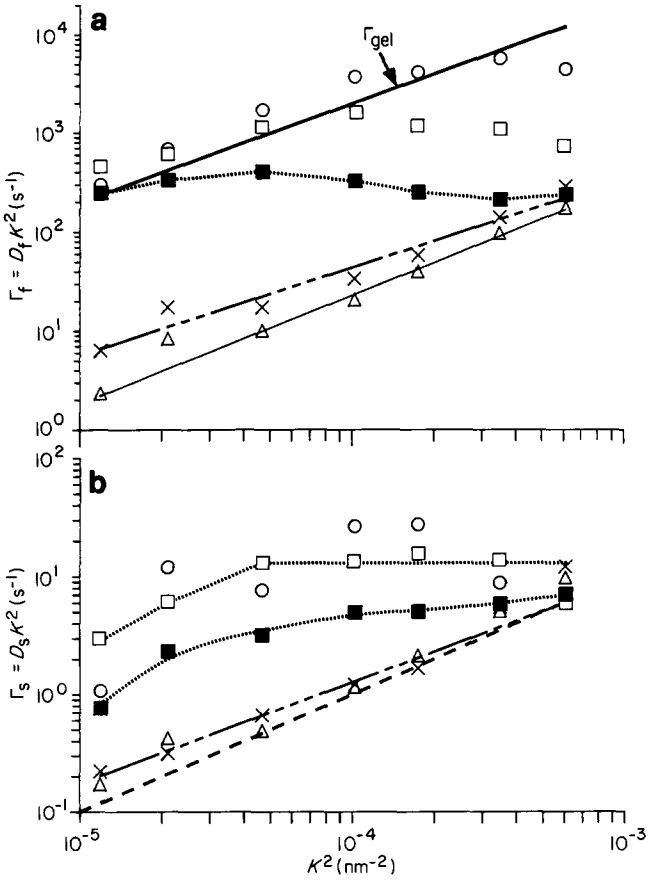

Figure 5 $\mathbf{K}^2$ dependence of the decay rates for different f_{Bis} corresponding to the different regions with respect to gelation with 50 nm probe. (a) ———, $\mathbf{K}$ dependence of the measurements for a 5% gel without probes; —···—, a fit to the data for the gel threshold sample and shows that $\mathscr{D}_f$ is itself $\mathbf{K}$ dependent, $\mathscr{D}_f \sim \mathbf{K}^{1.5}$. For comparison the dashed line of slope 1 corresponding to $\mathscr{D}_f \sim \mathbf{K}^2$ is also shown. The pre-gel threshold sample ($f_{Bis} = 1.4\%$) is consistent with $\mathscr{D}_f \sim \mathbf{K}^2$ whereas the post-gel threshold sample ($f_{Bis} = 1.6\%$) is not. The dotted lines are simply to guide the eye. (b) This shows the corresponding $\mathbf{K}$ dependence of the slow mode. In (a) and (b) f_{Bis}: △, 1.4%; ×, 1.6%; ■, 2.0%; □, 3.0%; ○, 5.0%

provided η is interpreted as the microscopic viscosity felt by the probe. Thus, the decrease of Γ and consequently $\mathscr{D}$, for fixed $\mathbf{K}$, with increasing f_{Bis} (see *Figure 4a*) is due to a 100-fold increase of microviscosity as we approach the gel point from below. In fact the data is consistent with $\mathscr{D}_s$, $\mathscr{D}_f \approx (f_{Bis}^c - f_{Bis})^\alpha$, where $\alpha = 0.8$ to 1.0. This value of α is comparable to the values observed in macroscopic measurements of viscosity η, at the sol–gel transition, where η scales as $(p_c - p)^{-\alpha}$ with p being the bond probability in percolation[18]. Note that $(f_{Bis}^c - f_{Bis})$ plays the same role as $(p_c - p)$. As f_{Bis} gets close to f_{Bis}^c the single exponential fits become somewhat poorer and a double exponential fits the data better. The decay constant of the slower mode of the double exponential fits, Γ_s, is very close to the value obtained from the single exponential fits and the cumulant analysis. Thus Γ_s represents the mode characteristic of the diffusion motion of the probes in the pre-gel.

We observed that the difference between the two decay rates gets smaller for decreasing f_{Bis} below f_{Bis}^c and that in region I the slow diffusion mode is the dominant mode. There are several possible interpretations for the appearance of the fast mode Γ_f in region I. One possibility is that the broadening of the distribution of decay rates comes from a spread of microviscosities due to a wide distribution of low molecular weight branched polymeric molecules formed prior to the formation of the incipient gel cluster. Another possible interpretation of the presence of a small amount of the fast mode could be from a dynamic coupling between the probe movement and the diffusion of the polymer in the semidilute solution. Such an interpretation is similar to the coupling mode seen in the ternary system of polymethylmethacrylate, polystyrene and toluene[19].

In region II the single exponential fit is very poor and a clear bimodality is observed in the exponential sampling analysis (cf. *Figure 3*). The slow mode Γ_s is closer to the effective decay constant, obtained from the first cumulant and as seen in *Figure 4a*, it goes over the value in the pre-gel state as f_{Bis} decreases. Thus this mode can be identified as arising from the translational movement of the probes in the gel.

The decay constant Γ_s is lowest at the gel threshold ($\Gamma_s \approx 2.83\ s^{-1}$ corresponding to an effective diffusion constant of $\sim 0.8 \times 10^{-10}$ cm^2/s). Γ_s appears to have a complex dependence on size. Only in the pre-gel samples is there a size dependence of the diffusion constant of the slow mode which agrees with the Stokes–Einstein relation. However at the vicinity of the threshold there appears to be some departure. For well gelled samples ($f_{Bis} > 2\%$) the experimental error in Γ_s is too large to determine the size dependence with any degree of confidence because here we have restricted ourselves to only 50 and 100 nm probes.

The $\mathbf{K}$ dependence of the slow mode (see *Figure 5b*) depends on the values of f_{Bis}. For samples close to f_{Bis}^c, $\Gamma_s \sim \mathbf{K}^{2-\Xi}$, implying that the latex probes essentially move as Brownian particles but that the diffusion coefficients are slightly $\mathbf{K}$ dependent. However for $f_{Bis} > 2\%$, Γ_s is essentially independent of $\mathbf{K}^2$, except at low values of $\mathbf{K}$.

To explain these observations we suggest an interpretation based on the structure of the polyarrylamide gels. At f_{Bis}^c the concentration of crosslinks is just enough to form the infinitely connected polymer cluster, however the pore size, ξ_{mesh}, inside the gel is very large with respect to the diameter of the probes used in this study ($\xi_{mesh} \gg d$). (Strictly speaking at the gel point $\xi_{mesh} \to \infty$.) Thus most of the particles are still capable of diffusing. After the onset of gelation a further increase of the crosslink content causes the formation of a fine mesh or smaller pores in the gel phase. The structure of a gel is quite likely to be non-homogeneous, with both a large interconnected space and small pores whose distribution is likely to be continuous and quite wide. It is also possible that there exist regions of higher crosslink density interwoven into the large interconnected void space[20]. As f_{Bis} increases ξ_{mesh} and the width of the mesh size distribution decrease. With this picture in mind the movement of the probe particles can be broadly classified into three categories:

(1) Particles moving in the large interconnected regions
(2) Particles moving inside pores whose size ξ_{mesh} is of the order of a few particle diameters, or in a temporal sense, particles spend some fraction of their total transit time through the gel in regions of higher crosslinking density
(3) Particles trapped in pores of size comparable to the diameter of the particle.

Clearly the relevant parameter here is ξ_{mesh} as it

approaches d, the diameter of the probe. Corresponding to these three types of environments there are three different dynamical behaviours possible. These are discussed below.

Almost free diffusion

When particles move in the large interconnected space outside the fine gel mesh they are diffusing essentially freely and hence have few encounters with the network. The volume fraction of this interconnected space is quite large at the gel point and decreases as the amount of crosslinks increases. This more or less free Brownian diffusion is seen clearly in the $f_{Bis}=1.6\%$ sample in the immediate vicinity of the gel point. For this sample the mode, Γ_s is diffusional, i.e. $\Gamma_s \propto \mathscr{D}(\mathbf{K})\mathbf{K}^2$. The diffusion coefficient appears to be slightly dependent on $\mathbf{K}$. In fact the data are consistent with $\mathscr{D}(\mathbf{K}) \sim \mathbf{K}^{-0.5}$. The $\mathbf{K}$ dependence implies that the diffusion coefficient depends on the length scale over which the particles move. If one uses the Stokes–Einstein equation, one would have to allow η, representing the viscosity of the sol fraction, to have a spatial dependence. As the extent of crosslinks increases the sol fraction decreases and thus the apparent diffusion coefficient $\Gamma_s/\mathbf{K}^2$, of these particles will increase with increasing f_{Bis}. This result is consistent with the result of Altenberg and Tirrel[21] who calculated the diffusion of particles through a randomly distributed system of fixed obstacles and found that the diffusion coefficient increases as the concentration of obstacles increases.

This free diffusional behaviour will only be seen provided $\mathbf{K}\xi_{mesh} < 1$. Because ξ_{mesh} decreases with increasing f_{Bis}, it is clear that at higher f_{Bis} free diffusional behaviour would be seen at lower $\mathbf{K}$.

Relaxational dynamics from particles in cages

If ξ_{mesh} is still large compared to the particle size but $\xi\mathbf{K} \approx 1$, then the dynamic light scattering is probing essentially only the local movement of the particles inside the pores of the gel. This type of behaviour can be modelled by considering the Brownian movement of a harmonically bound particle in a cage[22,23]. In this case the dynamics are characteristic of relaxational behaviour with Γ independent of $\mathbf{K}^2$, as long as $\xi_{mesh} > 1/\mathbf{K}$. Γ depends on the cage size (ξ_{mesh}), becoming larger as the cage size decreases, hence Γ_s increases as f_{Bis} increases. Γ also depends on the ratio E/f where E is the longitudinal elastic modulus of the gel network and f the friction due to the solvent. This relaxational behaviour is clearly seen in the $f_{Bis}=2\%$ sample with 50 nm probes for $\mathbf{K} > 4.4 \times 10^{-3}\ \text{nm}^{-1}$. For this sample as well as the $f_{Bis}=3\%$ sample a gradual crossover between almost free diffusion at small $\mathbf{K}$ to relaxational dynamics at larger $\mathbf{K}$ is observed for the slow decay modes. For the 50 nm probes the crossover occurs around $\xi_{mesh} \approx 200$ nm for the 2% sample, and around ~ 150 nm for the 3% sample. Thus the crossover occurs at smaller values of $1/\mathbf{K}$ as f_{Bis} increases and thereby ξ_{mesh} decreases. For a larger particle one expects the relaxational behaviour to extend to lower $\mathbf{K}$, because the finite size of the particles decreases the available space in which the probes can move. This was observed in our experiment with the 100 nm probes, where no crossover to diffusional behaviour could be observed up to the smallest value of $\mathbf{K}$ measured in this experiment ($3.45 \times 10^{-3}\ \text{nm}^{-1}$).

Coupling of gel and probe motions

So far we have discussed the slow mode. We now address the question of what is the origin of the fast mode. As can be seen from *Figure 4* the magnitude of the fast mode Γ_f increase very rapidly with increasing f_{Bis} varying from $10^2\ \text{s}^{-1}$ at the threshold to eventually becoming $5 \times 10^3\ \text{s}^{-1}$ in the well gelled samples. Because Γ_f for $f_{Bis} > 2\%$ is larger than the value of $\mathscr{D}_0\mathbf{K}^2$ where $\mathscr{D}_0$ is the diffusion constant of latex particles in aqueous suspension, it is clear that the mode cannot be directly ascribed to the translational diffusional movement of the probe particles in the gel. At $f_{Bis}=5\%$ the value of Γ_f practically coincides with Γ_{gel}, the value of the decay constant characteristic of the collective diffusion mode of the gel network[24] ($\sim 2 \times 10^{-7}\ \text{cm}^2\ \text{s}^{-1}$) measured on a polyacrylamide gel with total monomer concentration of 2.5% and $f_{Bis}=5\%$ without any latex particles added. In order to get appreciable scattering from this weak gel the measurements were made with an argon ion laser with a power at the sample of ≈ 300 mW, in contrast to the measurements from latex probes in gels which were done with a He-Ne laser (maximum power 15 mW) because of the high scattering from the latex particles. However as seen in *Figure 4a* Γ_{gel} decreases only slightly with f_{Bis} (similar results were observed by Geissler and Hecht[25] on the effect of varying crosslink content on polyacrylamide gels) whereas Γ_f decreases by an order of magnitude over the same range of f_{Bis}.

There are two possible interpretations of the fast mode. In the first Γ_f is itself the collective mode Γ_{gel} whose relative contributions are amplified via heterodyning with the trapped particles acting as local oscillators. Although this is possible at $f_{Bis}=5\%$ it seems unlikely to be the case at low f_{Bis} because $\Gamma_f \ll \Gamma_{gel}$. In the second Γ_f results from a dynamical (mechanical) coupling between the motion of the particle and the network mediated via the solvent. One way to visualize this is to consider the trapped particles, i.e. particles in these cages where $\xi \approx d$, such that their movement will be coupled to that of the gel, resulting in a fast mode whose frequency will lie between the slow and the collective gel modes. It is quite plausible that at low crosslinking this coupling would be weak because cage size is large and both the number of trapped particles and the frequency of interaction between the probes and the network are small. Therefore the frequency Γ_f will be closer to that of the particle rather than that of the gel. This coupling interpretation is further substantiated by the fact that Γ_f is almost independent of size for $f_{Bis} > f_{Bis}^c$.

The $\mathbf{K}$-dependence of Γ_f is complicated because it reflects the motion of both the gel and the particles and is dominated by which of the two contributes more strongly to the dynamic light scattering. For the very well gelled samples a very large fraction of the probe particles are completely trapped in pores of size comparable to the particle size. Such completely immobilized particles will not directly produce any dynamic light scattering, so that the dynamic light scattering from the gel itself becomes an important contribution. Tanaka *et al.*[22] showed that the decay rate, Γ_{gel}, for a polyacrylamide gel is proportional to $\mathbf{K}^2$, i.e. $\Gamma_{gel} = \mathscr{D}_{gel}\mathbf{K}^2$, where $\mathscr{D}_{gel}$ is the collective diffusion coefficient of the gel. *Figure 5a* shows values of the Γ_{gel} for a $f_{Bis}=5\%$ gel without probes, and we observe Γ_f for the 5% gel with probes to coincide with Γ_{gel}. Moreover, for this sample $\Gamma_f \propto \mathbf{K}^2$. We also find that for the samples

with $f_{Bis}=2\%$ and 3% at low **K**, $\Gamma_f \propto \mathbf{K}^2$ and coincides with the collective diffusion mode of the gel. This occurs because the intensity of the dynamically scattered light from the locally moving particles is strongly **K**-dependent and decreases significantly as $\mathbf{K} \to 0$. On the other hand, the intensity scattered by the collective diffusion mode of the gel is independent of **K** and thus for low **K** the scattering from the gel cannot be neglected. Unlike the 2% and 3% samples where the collective diffusion of the gel could only be observed at low values of **K**, for the 5% sample, where the dynamic scattering from the particle is only about 10%, the fast mode coincides with collective mode of the gel at all values of **K**. Also note that in this case where the scattering from the gel becomes comparable to that from the particles, heterodyning of the two signals is possible and can explain the differences between the measurements of $\mathscr{D}_{gel}$ for a pure gel sample *versus* the apparent $\mathscr{D}_{gel}$ obtained from the gel plus probes sample. At high **K**, for the 2% and 3% gels, Γ_f is independent of $\mathbf{K}^2$ and reflects the fact that the scattering from the particles is the dominant contribution.

The ratio of the amplitudes of the fast *versus* the slow mode depends both on **K** and f_{Bis}. For most of the samples the dominant mode is the slow mode (i.e., $A_f/A_s<1$) when $f_{Bis}<f_{Bis}^c$. The ratio of the amplitudes A_f/A_s in the double exponential fit appears to increase with increasing f_{Bis}. As f_{Bis} increases the distribution of pore sizes shifts to smaller values. Thus the number of particles moving in smaller cages will increase at the expense of those moving in larger cages and consequently the ratio A_f/A_s increases with increasing f_{Bis}. For the 5% sample the ratio A_f/A_s actually becomes greater than one, because of the contribution of the collective diffusion mode of the gel to the fast mode.

CONCLUSIONS

Our results demonstrate that probe dynamics is governed by quite different mechanisms in solutions and gels. Below the gel threshold the dynamical behaviour is diffusional and the diffusion constant decreases as the microviscosity of the sample increases as it approaches the gel point. Above the gel threshold the dynamical behaviour is different on different length scales over which the probes move.

The latex probes of diameter d will exhibit three different types of behaviour according to the size ξ, of the 'cage' which they may occupy. For ξ much greater than d, $\Gamma \propto \mathbf{K}^{2-\Xi}$, where Ξ is an exponent (of the order of 0.5). It appears that Ξ depends on f_{Bis}. The probes undergo a diffusion which is mostly translational and the diffusion constant depends on the viscosity of the sol phase. For ξ only slightly greater than d, (mesh size of the order of a few particle diameters), Γ is independent of $\mathbf{K}^2$. The probes move in a finite size 'cage' and exhibit mostly a relaxational behaviour similar to that of a particle harmonically bound by a flexible 'cage'. For $\xi \approx d$, $\Gamma \propto \mathbf{K}^2$. The probes are completely immobilized and the intensity of the dynamic scattering from the probes decreases. The faster mode, which is either due to the coupling of the motion of the probes and the gel or due to the motion of the gel itself amplified via heterodyning with the trapped probes, becomes more evident at higher f_{Bis} values. Consequently, the particles act as local probes which can be used to study the elasticity of the gel network.

ACKNOWLEDGEMENTS

This research was supported by a grant from National Science Foundation and the Gillette Company. We thank R. Molnar, I. Segall, and D. Russell for their technical assistance.

REFERENCES

1 Havlin, S. and Ben-Avraham, D. *Adv. Phys.* 1987, **36**, 695
2 Lin, T. H. and Phillies, G. D. J. *Coll. Int. Sci.* 1984, **100**, 82
3 Russo, P. S. *Macromolecules* 1985, **18**, 2733
4 Rymden, R. and Brown, W. *Macromolecules* 1986, **19**, 2942
5 Chu, B. 'Laser Light Scattering', Academic Press, New York, 1974
6 Phillies, G. D. J., Ullman, G. S., Ullman, K. and Lin, T. H. *J. Chem. Phys.* 1985, **82**, 5242 and references therein
7 Allain, C., Drifford, M. and Gauthier-Manuel, B. *Polymer* 1986, **27**, 177
8 Madonia, F., San Biagio, P. L., Palma, M. U. *et al. Nature* 1983, **302**, 412
9 Nishio, I., Reina, J. C. and Bansil, R. *Phys. Rev. Lett.* 1987, **59**, 684
10 Bishop, M. T., Langley, K. H. and Karasz, F. E. *Phys. Rev. Lett.* 1986, **57**, 1741
11 Langevin, D. and Rondelez, F. *Polymer* 1978, **19**, 875
12 Reina, J. C. *PhD Thesis*, Boston University, USA, 1989
13 Maurer, H. R. 'Disk Gel Electrophoresis', de Gruyter, Berlin, *1971*
14 Ostrowsky, N., Sornette, D., Parker, P. and Pike, E. R. *Optica Acta* 1981, **28**, 1059
15 Stock, R. S. and Ray, W. H. *J. Polym. Sci., Polym. Phys. Edn* 1985, **23**, 393
16 Oliver, C. J. In 'Photon Correlation and Light Beating Spectroscopy' (Eds H. Cummins and E. R. Pike), Plenum Press, New York, 1974, pp. 151–223
17 Bloomfield, V. A. and Lim, T. K. *Meth. Enzymol.* 1978, **48**, 415
18 Stauffer, D., Coniglio, A. and Adam, M. *Adv. Polym. Sci.* 1982, **44**, 103
19 Chu, B. and Wu, D.-Q. *Macromolecules* 1987, **20**, 1606
20 Hsu, T. P. and Cohen, C. *Polymer* 1984, **25**, 1419
21 Altenberg, A. R. and Tirrel, M. *J. Chem. Phys.* 1984, **80**, 2208
22 Dalberg, P. S., Bøe, A., Strand, K. A. and Sikkeland, T. *J. Chem. Phys.* 1978, **69**, 5473
23 Wang, M. C. and Uhlenbeck, G. E. In 'Selected Papers on Noise and Stochastic Processes' (ed. N. Wax), Dover, New York, 1954
24 Tanaka, T., Hocker, L. O. and Benedek, G. *J. Chem. Phys.* 1973, **59**, 5151
25 Hecht, A. M. and Geissler, E. *J. Physique* 1978, **39**, 631